Effect of inclination angle on hooked end steel fiber pullout behavior in ultra-high performance concrete

Composite Structures 201 (2018) 151–160

Contents lists available at ScienceDirect

Composite Structures

journal homepage: www.elsevier.com/locate/compstruct

Effect of inclination angle on hooked end steel fiber pullout behavior in ultra-high performance concrete

Y.Y.Y Cao, Q.L. Yu*

Department of the Built Environment, Eindhoven University of Technology, P.O. Box 513, 5600 MB Eindhoven, the Netherlands

ARTICLE INFO

Keywords:
Single-fiber pullout
Hooked end fiber
Ultra-high performance concrete
Inclination angle
Parametric evaluation
Pullout mechanism

ABSTRACT

The bond relationship between the concrete matrix and steel fiber is a significant factor that affects the performance of ultra-high performance fiber reinforced concrete (UHPFRC). In the present research, pullout performances of hooked end fibers embedded in ultra-high performance concrete matrix under various inclination angles are systematically investigated, with special attention on fiber dimension and embedded length. Pullout load-slip curves are obtained and experimental observations including complete fiber pull-out, fiber rupture and matrix failure are analyzed in detail. The effects of the pullout angle are then studied quantitatively by parameter calculations and mechanism analysis. A new analytical model for evaluating the snubbing and spalling effects of the hooked end steel fiber is proposed and validated. It is shown that the influences of the inclination angle on the peak pullout load vary with different fiber types, embedded lengths and fiber diameters, which are also associated with the occurrences of the fiber rupture and the matrix failure. In addition, optical microscope and scanning electron microscopy observations at mesoscale are performed to further analyze the effects of orientation angle.

1. Introduction

Ultra-High Performance Fiber Reinforced Concrete (UHPFRC) is a construction material characterized by its very high compressive strength, excellent durability, energy absorption capacity and damage tolerance [1–6]. Fibers play an important role in UHPFRC. The incorporation of fibers to ultra-high performance concrete (UHPC) matrix significantly improves its tensile strength, post-cracking ductility and energy absorption capacity, as well as reduces crack width and crack spacing [7–9]. In addition to the fiber content, individual pullout behavior of the activated fibers crossing a crack is also a significantly influential factor that affects the performances of UHPFRC composites.

As a foundation to analyze the fiber effects on cementitious composite and the fiber-matrix bond relationship, fiber pullout test provides basic information and a comprehensive understanding on the bond-slip characteristics, and thus enables further improvement on the fiber-matrix interfacial properties [10,11]. The pullout behavior of a single steel fiber depends on many factors [12], including the fiber geometry, orientation angle, embedded length, matrix quality, as well as the pullout rate. A number of pullout tests about fiber embedded in normal concrete (NC) or high strength concrete (HSC) have been performed, analytical and numerical models are also developed to predict the pullout load-displacement relationship [13]. However, since matrix quality is one dominant factor that influences the pullout behavior, the performance of steel fibers embedded in UHPC matrix can differ remarkably with that in NC or HSC [10,12,14]. Fig. 1 plots the load-slip relationships of a smooth straight fiber pulled out from NC and UHPC matrix [14,15]. Instead of a sudden sharp drop after reaching the peak stress as observed in the case of NC (Fig. 1a), the pullout stress of UHPC declined continuously until the end of the complete pullout process (Fig. 1b). As indicated by scanning electron microscope (SEM) images, the fiber-matrix interface zone of the UHPC matrix is much denser than that of NC and HSC thanks to the usage of fine particles and the improved filling effect in UHPC [10,16]. The high particle packing density of UHPC matrix creates a superior bond between the fiber and the matrix, leading to a slip-hardening pullout phenomenon that is not encountered in the NC matrix [10]. The enhanced strength of the matrix also provides a higher resistance to the matrix spalling, hence increasing the fiber's capabilities in the pullout resistance and energy absorption [17]. In addition, as the water/binder (W/B) ratio is reduced in UHPC, its shrinkage magnitude is enhanced. It should be noted that concrete shrinkage has both positive and negative effects on the interfacial bond: (1) the higher radial confinement pressure generated due to shrinkage benefits the enhancement of friction bond; (2) shrinkage stress can also result in matrix cracking, which weakens the fiber-matrix bond. By testing the influence of shrinkage reducing agent on the

* Corresponding author.
E-mail address: q.yu@bwk.tue.nl (Q.L. Yu).

https://doi.org/10.1016/j.compstruct.2018.06.029
Received 7 May 2018; Received in revised form 1 June 2018; Accepted 7 June 2018

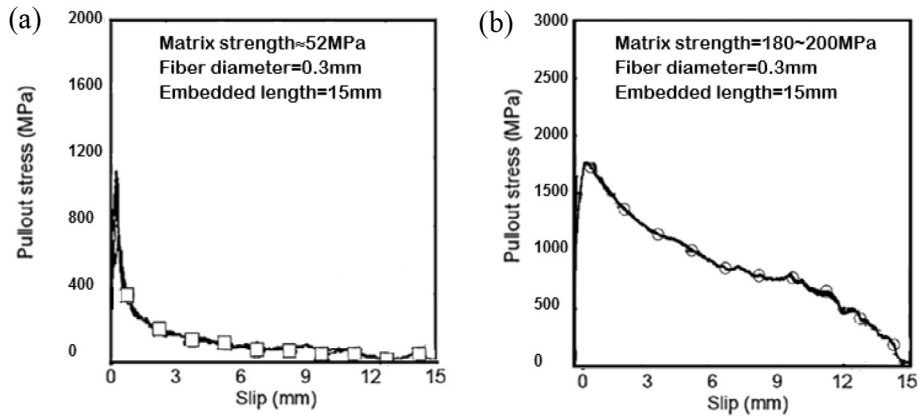

Fig. 1. Pullout stress versus slip of smooth straight fibers from: (a) NC [14]; (b) UHPC [15].

pullout performance of UHPC, [15] confirms that the shrinkage in UHPC has a more prominent effect on increasing the interface bond compared to the decrease caused by cracking.

Being a relatively new material [1–3], UHPFRC has been increasingly utilized in modern constructions in recent years. Nonetheless, studies about the pullout characterization of UHPFRC are still insufficient, especially compared with the investigations concerning NC and HSC [10,14]. Among the limited studies, Wille and Naaman [10,18–20] conducted a series of single fiber pullout tests of steel fibers embedded in UHPC matrix. The research reveals that the improvement in the particle packing of UHPC contributes to an enhanced bond slip hardening behavior. By comparing the pullout responses of the straight and the deformed fibers, they found that the complementary mechanical bond of the deformed fiber increases the equivalent bond strength. However, these enhanced bond properties also lead to the breakage of the fiber during the pullout process. Abdallah et al. [11] analyzed the fiber-matrix interfacial properties of hooked end steel fibers embedded in UHPC matrixes with various fiber embedded lengths and W/B ratios. Their results present that the maximum pullout load increases as the W/B ratio decreases, while the embedded length has no appreciable effect. Yoo et al. [16,21] investigated the influences of fiber type and matrix strength on the pullout response of high performance fiber-reinforced concrete. They reported that the fiber pullout behavior is improved with the enhancement of the matrix strength, and the hooked end fibers exhibit higher bond strength and pullout work than the straight fibers.

In UHPFRC, fibers are usually randomly distributed. Fibers under different inclination angles provide distinct contributions at a given crack width [22]. On the one hand, fiber inclination can lead to increases in the bridging force and the pullout work [12,23]. On the other hand, it also generates higher stresses in the fiber and matrix, and thus a higher fiber and/or concrete rupture potential [12,23–25]. The analytical model developed by Zhang and Li [24] for studying the effects of inclination angle exhibits that fiber rupture load is significantly reduced for inclined fibers than for aligned ones, and this load decreases with the increment of the matrix modulus. It can be inferenced from their research that steel fibers embedded in a high-modulus UHPC matrix with inclination angles other than 0° may have higher chances to break during the pullout processes. This further indicates the importance of studying the effects of inclination angle on the pullout behavior from UHPC. Nonetheless, most of the current pullout investigations regarding UHPC focus on aligned fibers while research concerning inclined fibers is inadequate. Lee et al. [26] conducted pullout tests of straight steel fibers embedded in UHPFRC with orientation angles of 0 to 60°, the largest peak load is observed at an angle between 30 and 45°. Xu et al. [27] studied the pullout behaviors of straight steel fibers from UHPC and analyzed the influences of inclination angles on the loading rate sensitivity. It is found in their research that an inclination angle of 20° leads to a more promising rate effect. More recently, Tai and El-Tawil [28] investigated the pullout behaviors of inclined deformed steel fibers in UHPC under different loading rates. According to their study, pullout resistances are sensitive to both inclination angle and loading rate. However, their study focused more on the loading rate effect rather than the influence of the pullout angle.

Since traditional UHPFRC is usually reinforced with straight steel fibers in order to match the fine aggregates in the UHPC matrix, the objectives of most pullout research about UHPC are usually smooth straight fibers [29]. However, recent researches show that concrete containing appropriate type and content of coarse aggregate possesses some advantages on e.g. economic efficiency, shrinkage control [30] and impact resistance improvement [31,32]. For these UHPFRC with coarse aggregates, e.g. large basalt aggregates, hooked end steel fiber is a more appropriate and efficient reinforcement considering its stronger crack-bridging effect [33]. In addition, hooked end steel fibers are increasingly used in UHPFRC to enhance the interfacial bond [1,34–39]. Some investigations confirm that UHPFRC composite reinforced with deformed steel fiber, e.g. hooked end fiber or twisted fiber, provides a superior performance with respect to post cracking strength, strain capacity and multiple cracking behavior than its counterpart with straight fiber [33,37–39]. These tendencies make understanding the pullout behavior of hooked end fibers embedded in UHPC matrix of great significance. To investigate the pullout responses of inclined fibers, analytical models for evaluating the combined effects of snubbing and matrix spalling are of great importance [26]. Despite the models for straight steel fibers [17,26,28], there is still a lack of theoretical model for hooked end fibers. Furthermore, the insufficiency of researches concerning the performances of inclined hooked end fibers pulled out from UHPC matrix also highlights the significance of conducting systematical investigations.

Accordingly, the present study aims to investigate the pullout performances of hooked end steel fibers embedded in an UHPC matrix, with the effort on the effects of inclination angles. Single fiber pullout tests are performed, supported by mechanical parameter calculations. Based on equations for straight fiber pull-out, a new theoretical model for hooked end fibers to evaluate the snubbing and matrix spalling effects is developed. Furthermore, mesoscale observations of the investigated materials are carried out employing optical microscope and SEM. The results obtained from this study provide fundamental insights on the effect of hooked end steel fibers for improving UHPFRC properties and for a more efficient utilization of fibers in UHPFRC.

2. Single fiber pullout experiments

2.1. Steel fibers

As shown in Fig. 2, two types of hooked end steel fibers are used in the single fiber pullout tests in the present study. One is a commercially

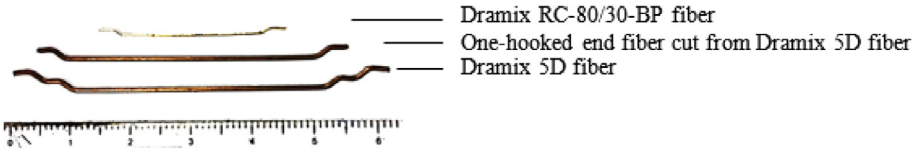

Fig. 2. Hooked end steel fibers in the single fiber pullout tests.

Table 1
Specifications of fibers.

Fiber type	Dramix RC-80/30-BP fiber	One-hooked end fiber cut from Dramix 5D fiber	
Identification	H-0.38-10	H-0.9-10	H-0.9-15
Fiber diameter d (mm)	0.38	0.90	0.90
Fiber length l_f (mm)	30	60	60
Embedded length l_e (mm)	10	10	15
Tensile strength f_t (MPa)	2600	2600	2600

available steel fiber, i.e. Dramix RC-80/30-BP fiber, and the other one is a one-hooked-end steel fiber cut from Dramix 5D fiber. The basic geometry and mechanical parameters of the fibers are given in Table 1. The identification is defined as follows: the first letter indicate the fiber is hooked end steel fiber, the first number denotes the fiber diameter in mm, and the last number indicates the fiber embedded length in mm. For example, H-0.38-10 is a hooked end fiber with a diameter of 0.38 mm embedded with 10 mm.

2.2. UHPC matrix

The UHPC matrix for the pullout test is based on the recipe described in Li et al. [40]. The raw materials used are Portland Cement CEM I 52.5 R (PC), micro-silica (mS), limestone powder (LP), sand 0–2 (S), basalts aggregate 1–3 (BA), water (W), and PCE-type superplasticizer (SP). The particle size distributions of the materials are measured by sieve and laser diffraction analyses (Malvern Mastersizer 2000®), as shown in Fig. 3. Tables 2 and 3 give the specific densities and proportions of the materials used in the UHPC matrix, respectively [40]. The average compressive strength f_c of the UHPC measured at 28 days is 156 MPa. More detailed information about the mix design, mechanical properties and followability of the UHPC matrix can be found in [40].

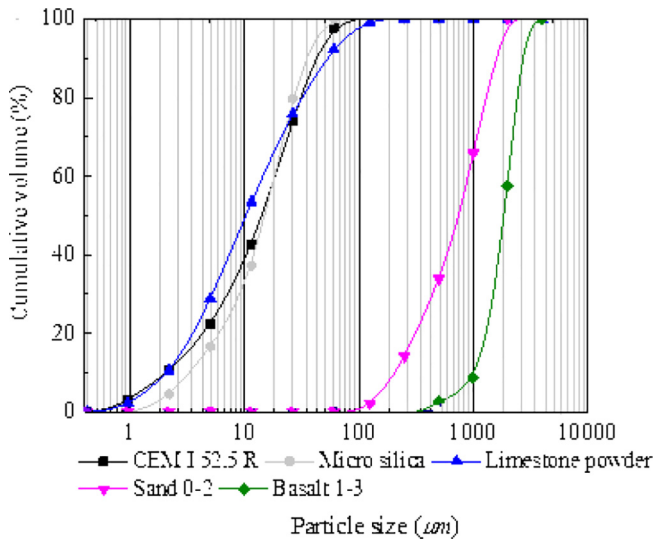

Fig. 3. The particle size distribution of raw materials [40]

Table 2
Specific densities of raw materials (g/cm^3) [40].

Materials	PC	mS	LP	S	BA	W	SP
Specific density	3.15	2.32	2.71	2.72	3.05	1.00	1.07

Table 3
Recipe of UHPC matrix (kg/m^3).

Materials	PC	mS	LP	S	BA	W	SP
Quantity	675	45	180	864.5	576.3	180	10.8

2.3. Casting of specimens

The following mixing procedure is adopted for the preparation of the UHPC matrix: dry mixing for 2 min with all powder, sand and basalt aggregates; adding 75% water and mixing for 2 min; sequentially adding the remaining water with the superplasticizer incorporated and mixing for another 2 min at a low speed and then 4 min at a high speed. The mixing procedure is conducted at room temperature of about 20 ± 1 °C. After mixing, the self-consolidating UHPC is poured without vibration into a half dog-bone shape mold, in which a single hooked end fiber is carefully placed and held by hard foams with the desired embedded length and inclination angle (Fig. 4a and b). The inclinations applied in this study are 0°, 10°, 20° and 30°. At least five specimens are tested in each inclination category. After casting, the specimens are covered with plastic sheets to prevent moisture evaporation and stored at room temperature for 24 h. Then they are demolded and cured in water under room temperature for an additional 27 days. All specimens are tested in surface dry condition after the age of 28 days.

2.4. Pullout test setup and procedure

The pullout test is conducted using an Instron 5967 universal testing machine (Fig. 4c). A round concrete grip is applied to hold the half dog-bone shaped specimen in order to reduce the confinement effect of the grip on the concrete. The fiber grip is also specially designed such that the free end of the fiber is tightly held without significant slippery in the grip. By assuming that the elastic deformation of the steel fiber and the grips are small enough [16,19,27,32], the fiber slip is measured according to the vertical movement of the grip system. The pullout load is measured by a load cell with a capacity of 30 kN. The tests are performed under the displacement control and the pullout rate adopted is 0.5 mm/min.

3. Pullout responses

During the pullout tests three distinct responses are observed, namely complete fiber pullout, fiber rupture and matrix failure. The first one is usually observed under small pullout angles for the three categories. On the contrary, the second and third ones occur more frequently under larger inclination angles for the H-0.38–10 and H-0.9–10 fibers, respectively.

3.1. Complete fiber pullout

To analyze the complete pullout behavior, typical pullout load-slip

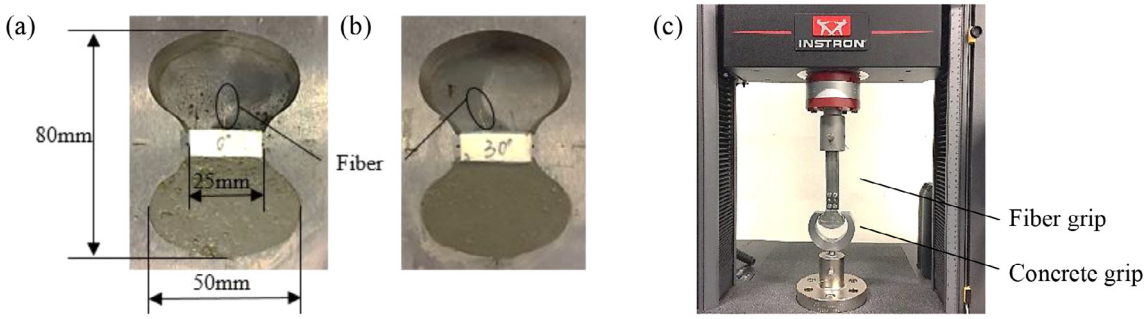

Fig. 4. Pullout specimens and test setup: (a) 0 °specimen; (b) 30 °specimen; (c) Instron testing machine.

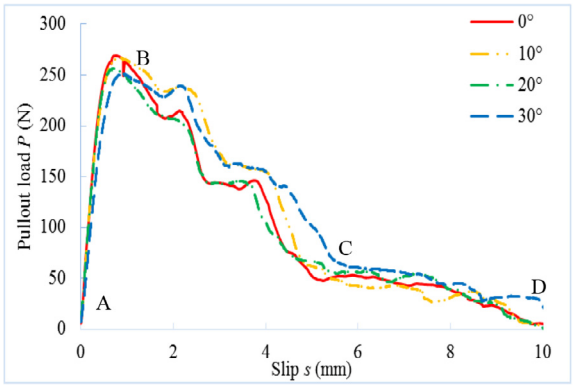

Fig. 5. Pullout load-slip curves of H-0.38-10 fiber.

Table 4
Number of fiber ruptured specimens and total tested specimens.

Angle (°)	0	10	20	30
H-0.38-10	0 out of 5	2 out of 7	2 out of 7	7 out of 10

relationships for the H-0.38-10 fiber under different angles are plotted in Fig. 5. The curves for each inclination angle are the average values of at least 5 specimens except for the 30° category, which is averaged from 3 specimens due to the fiber rupture of the other specimens (Table 4). As can be observed in Fig. 5, these curves have resemble shapes, suggesting a good alignment of the testing as well as a similar pullout process under different inclination angles. In the initial elastic stage of the pullout test, the response is almost linear until the initiation of debonding (point A), after which fiber–matrix interface failure begins. The pullout load then increases at a slower rate. The contribution of the hook is activated after the complete debonding of the fiber and it reaches its maximum at the peak point B. Through the pullout process in this stage, the hook part of the steel fiber undergoes large deformations, i.e. plastic hinges are formed in the two curved sections of the fiber hook where plastic bending occurs. In addition, the corresponding slip under point B increases with the increase of the orientation angle. Subsequently, the ascending slope of the pullout load–slip curve tends to be smaller under a larger angle. In the post-peak stage, the hook undergoes a straightening procedure, during which the plastic hinges play an important role. The fluctuations of the curve after point B are associated with the deformation of the hook. When the hook is fully straightened and slips along the straight tunnel (point C), the plastic hinges are deactivated and fiber-matrix friction becomes the dominant mechanism. The pullout load decreases gradually due to the reduction of the remained embedded length until the end of the pullout process (point D).

Fig. 5 also exhibits the effect of the orientation angle on the peak pullout load. The values under 0° and 10° are close to each other and

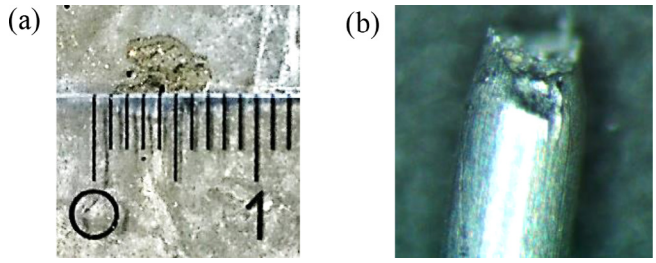

Fig. 6. Failures of matrix and fiber: (a) matrix spalling; (b) ruptured fiber.

they are only slightly higher than those under 20° and 30°. This is primarily due to some small concrete pieces spalling off from the pullout surface at 20 and 30°, resulting in a smaller embedded length of the steel fiber, thus a reduced pullout load. An example of the matrix spalling zone on the pullout surface under 30° is shown in Fig. 6a. The tendency in Fig. 5 is in accordance with the finding in [41] that the peak loads of the hooked end fiber remained nearly unchanged under angles from 0 to 60° when pulled out from a concrete with the compressive strength of 85 MPa. Nonetheless, contradictory results can be found in other literature. For example, Tai and El-Tawil [28] tested the pullout behavior of hooked end steel fiber from UHPC (f_c = 184 MPa) under 0 to 45° and found that the peak pullout load was maximized at approximately 30°. The difference may be ascribed to the following reasons. Firstly, the enhanced strength of the matrix in [28] can lead to an improved frictional resistance between the fiber and the matrix, generating a more remarkable snubbing effect that increases the peak pullout load with the inclination angle [25]. Secondly, in their test the spalling of matrix is only observed under the pullout angle of 45°, which means the resistance loss due to the reduced embedded length is only occurred under 45° rather than under 20 and 30° as observed in this study.

3.2. Fiber rupture

One common problem for pulling out an inclined fiber is its breakage. In this study, the majority of the H-0.38-10 fibers under 30° ruptured inside the matrix near the pullout surface. The numbers of specimens experienced fiber rupture are given in Table 4. An example of the ruptured H-0.38-10 fiber is shown in Fig. 6b, in which the irregular break surface and the reduced local cross-section area due to Poisson effect, i.e. necking, can be clearly observed.

During the pullout process, the fiber breaks when the localized strain is higher than its limit value or when the pullout resistance exceeds the ultimate tensile strength of the steel material. As suggested in [25], the yield of the steel fiber is the consequence of inter-crystal slippage in metal caused by atomic-level dislocation movements. In the case of inclined fibers, additional shear stress is imposed on the fiber where it enters the matrix. This additional stress considerably accelerates the inter-crystal slip within the crystal system of the fiber by lowering both its yield and ultimate strength. As a consequence, the

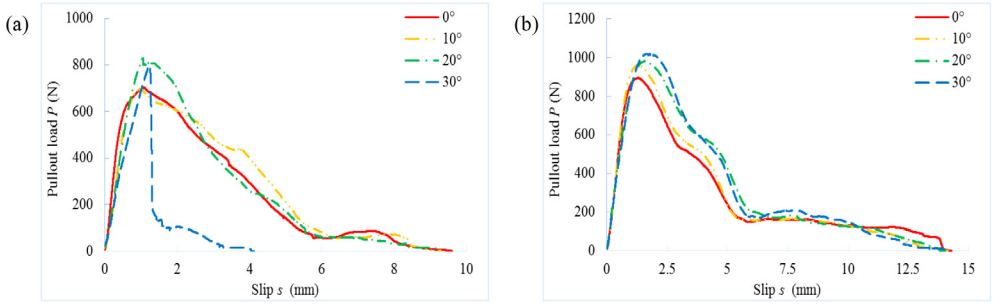

Fig. 7. Pullout load-slip curves: (a) H-0.9-10 category; (b) H-0.9-15 category.

inclined fiber would reach the ultimate conditions under a lower applied load. In other words, the fiber rupture load of an inclined fiber is reduced compared to its aligned counterpart, i.e. fiber apparent strength degradation occurs [24]. Since the degradation is more pronounced under larger angle, fibers loaded at a larger inclination angle exhibit a higher possibility to rupture during the pullout process.

3.3. Matrix failure

The pullout behavior of the H-0.9-10 fiber is illustrated in Fig. 7a. For this category, 20° is the optimum pullout direction to achieve the maximum peak pullout load. The curve of 30° has a sudden drop at a slip of about 1.8 mm because all the specimens tested under 30° have serious matrix failure. Fig. 8 shows examples of a failed matrix specimen and the H-0.9-10 fiber after the test under 30°. As the figure presents, the matrix is cracked from a location near the hooked end and the cracks propagate to the pullout surface, forming a crater inside the concrete. The depth of the crater is approximately the same as the embedded length of the fiber. As can be seen, the H-0.9-10 fiber is pulled out from the cracked matrix before the hook is straightened, which manifests that the contribution of the hook is not fully utilized. This matrix failure occurs more frequently with the increment of the pullout angle (Table 5).

One possible reason that leads to this matrix failure is the larger contact surface between the H-0.9-10 fiber and the matrix. Considering the larger diameter of the H-0.9-10 fiber, forces can be transferred more efficiently from the fiber to the matrix. Furthermore, the prominent anchorage force provided by the hook and the relatively small embedded length in the matrix also conduce to the matrix failure phenomenon. On the one hand, stresses at the bending regions of the hook due to slip shear and shrink-fit initiate the fracture of the matrix, making the matrix near the hook a weak region. On the other hand, the surrounding concrete matrix that covers the hook is too thin to resist the large anchorage force. This inappropriate combination of the large hook size and the small embedded length causes the matrix failure.

Increasing the embedded length of the fiber or adding micro fibers in the matrix are two potential methods to prevent the matrix failure. In this study, the former is utilized considering its simplification. The embedded length l_e is increased from 10 mm to 15 mm, i.e. the H-0.9-15 category. With this enlarged l_e, only one specimen has the matrix failure problem when it is pulled-out under 30°, none of the rest specimens encounters this problem. The pullout load-slip relationships for the H-0.9-15 category are plotted in Fig. 7b, in which increments of the peak pullout load are observed with the increase of the angle. Some characteristics that are observed in the H-0.38-10 category, e.g. the pullout slip under the peak load increases while the slope of the pre-peak branch of the curve decreases as the angle improves, still exist and even more obvious in this category. The increment of the slip can be ascribed to the matrix spalling that reduces the embedded length and allows fiber deformation. Moreover, the peak pullout load is also higher compared with that in Fig. 7a, thanks to the longer l_e.

Table 5
Number of matrix damaged specimens.

Angle (°)	0	10	20	30
H-0.9–10	1 out of 5	2 out of 5	4 out of 6	6 out of 6

4. Parametric evaluation and mechanism analysis

4.1. Evaluation of parameters for fiber pullout performance

To study the influences of the orientation angle on e.g. interfacial bond strength, pullout energy and fiber utilization efficiency, the following mechanical parameters are calculated. The maximum fiber stress $\sigma_{max}$is an important parameter to estimate the fiber utilization efficiency and predicts fiber pullout modes, i.e. pullout or rupture. It also gives reference to determine the minimum fiber strength needed to avoid fiber fracture. Assuming the bond strength is constant along the entire fiber embedded length, the equivalent bond strength τ_{eq} can be defined as the average bond strength based on the pullout energy dissipation, and it is associated with matrix cracking behaviors [15,16]. Moreover, the maximum bond strengthτ_{max}, related to the peak pullout load, is often used to evaluate the pullout resistances of fibers with different geometries [16]. Equations for calculating these parameters are:

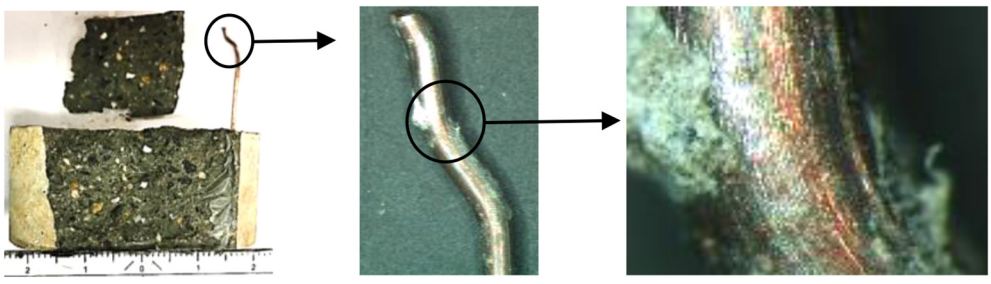

Fig. 8. Example of matrix failure and the fiber under 30°.

Maximum fiber stress: $\sigma_{max} = \frac{4P_{max}}{\pi d^2}$ (1)

Equivalent bond strength: $\tau_{eq} = \frac{2E}{\pi dL^2}$ (2)

Maximum bond strength: $\tau_{max} = \frac{P_{max}}{\pi dL}$ (3)

where P_{max} is the peak pullout load (MPa); E is the pullout energy dissipation and defined geometrically by the area below the pullout load-slip curve (N·mm); d is the diameter of the fiber (mm); and L is the actual fiber embedded length obtained from the pullout load-slip curves (mm).

Fig. 9 presents the angle effect on these mechanical parameters. The pullout energy, equivalent bond strength and maximum bond strength of the H-0.9-10 category under 30° are not given because of the serious matrix failure making the results incomparable. For the H-0.38-10 category, the listed parameters are almost independent of the inclination angle. This is quite distinct from the H-0.9-15 category, where improving the pullout angle can lead to increases of the parameters. By contrast, for the H-0.9-10 category, E and τ_{eq} are the highest under 10°, while other parameters achieve their maximum values under 20°.

In comparing these parameters for the H-0.38-10 and H-0.9-10 fibers, both P_{max} and E are improved with the larger fiber diameter. Nonetheless, the maximum fiber stress of the H-0.38-10 fiber (σ_{max} = 2255 MPa ~ 2436 MPa) is about twice larger than that of the other two categories, and it is close to the yield strength of the steel material (f_t = 2600 MPa), indicating a higher utilization efficiency of the smaller fiber. This larger σ_{max} also helps to understand the higher fiber breakage occurrence of the H-0.38-10 fiber in the pullout tests. Fig. 9c also plots that for the H-0.38-10 category, the aligned fiber or fiber with a small inclination angle achieves the highest fiber efficiency, while for the other two tested categories the fibers are better utilized under 30°.

Overall, in Fig. 9, τ_{eq} is the highest for the H-0.9-10 category, followed by the H-0.38-10 and H-0.9-15 categories, the ranges of their values are 19 MPa ~ 22 MPa, 16.5 MPa ~ 17.5 MPa and 14 MPa ~ 16.5 MPa, respectively. Since τ_{eq} is related with matrix cracking behaviors, the higher τ_{eq} for the H-0.9-10 category is in line with its more frequent matrix failure occurrence during the pullout tests. Moreover, τ_{eq} in this study with UHPC is much higher than its counterparts with NC and HSC, e.g. the values of τ_{eq} in [42] with the same fiber as the H-0.38-10 category embedded in NC (f_c = 28 MPa) and HSC (f_c = 84 MPa) are only 3.5 MPa and 4.7 MPa, respectively. τ_{max} is also the highest in the H-0.9-10 category, the values of which are between 26 MPa and 31.5 MPa. For the H-0.9-15 category, the maximum bond strength ranges from 22 MPa to 25.5 MPa, while for the H-0.38-10 fiber the values are around 21 MPa under the tested angles.

In addition, P_{max} and E are significantly improved for the hooked end fiber than the straight counterpart. For instance, P_{max} and E in [43] for aligned straight steel fiber (d = 0.2 mm, l_e = 5mm) pulled out from ultra-high strength concrete (f_c = 110 MPa) are only around 45 MPa and 120 N·mm. This confirms the advantages of hooked end fiber over the straight one and indicates its utilization potential in UHPFRC. Moreover, comparisons between the H-0.9-10 and H-0.9-15 categories

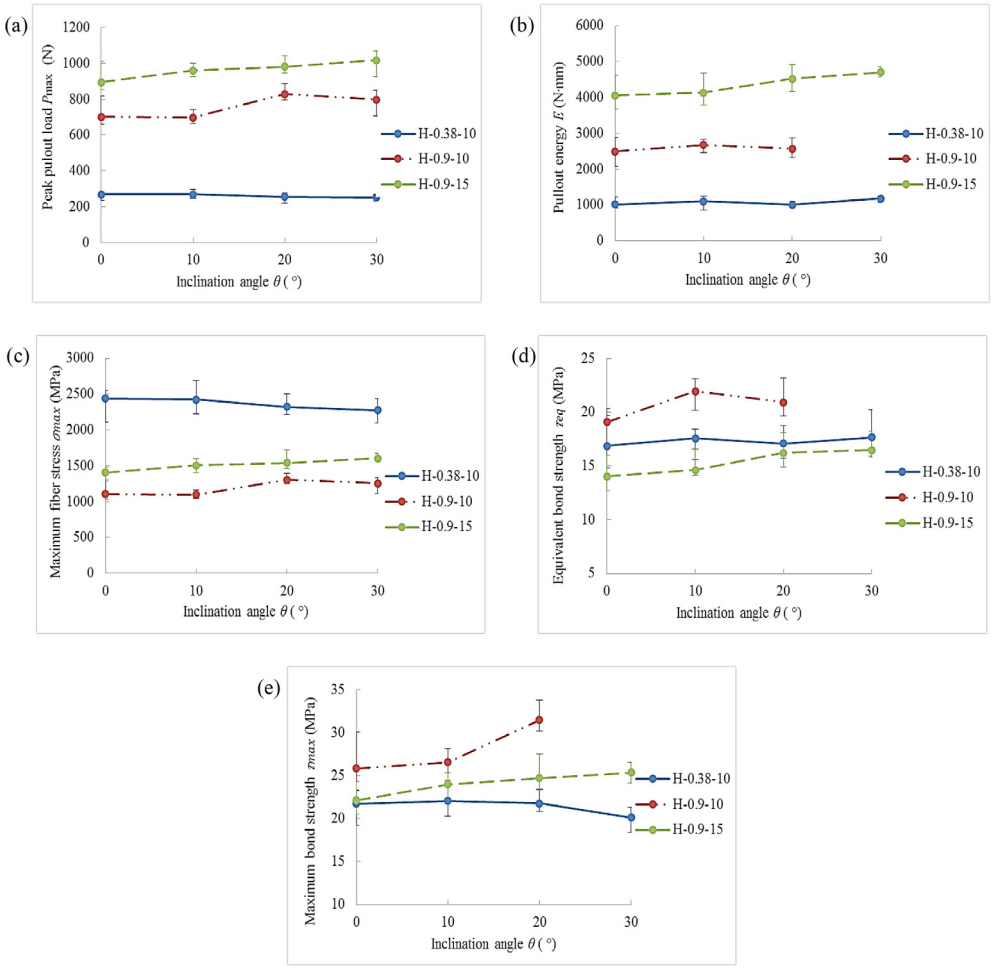

Fig. 9. Influences of angle on mechanical parameters: (a) peak pullout load P_{max}; (b) energy dissipation E; (c) Maximum fiber stress σ_{max}; (d) Equivalent bond strength τ_{eq}; (e) Maximum bond strength τ_{max}.

demonstrate that increasing the embedded length l_e of the fiber can efficiently enhance P_{max} and E, e.g. they increase 28% and 65%, respectively, when l_e increases from 10 mm to 15 mm. However, τ_{eq} and τ_{max} tend to be higher when l_e of the hooked end fiber is shorter, i.e. the averaged τ_{eq} and τ_{max} values of the H-0.9-10 category are approximately 38% and 18% higher than those of the H-0.9-15 category. This trend is also confirmed by comparing the results of the H-0.38-10 fiber under 0° with the ones in [15,32], which used the same fiber but different embedded lengths. Park et al. [15] analyzed the response of the aligned fiber with l_e = 15 mm pulled out from UHPC matrix (f_c = 180–200 MPa) and obtained that the values of τ_{eq} and τ_{max} are 7.5 MPa and 11.7 MPa, respectively. In [32], Tai et al. conducted similar tests with l_e = 6 mm and the UHPC matrix of 150 MPa. In their study, τ_{eq} and τ_{max} under 0° are 19.8 MPa and 23 MPa, respectively. This higher τ_{eq} and τ_{max} with smaller l_e of the hooked end fiber in turn manifests the more prominent contribution of the hook than the straight part of the fiber.

4.2. Snubbing and matrix spalling effect

The influences of fiber inclination on the pullout performance are associated with both the snubbing effect and the matrix spalling effect. The phenomenon that the pullout load increases with the increase of the inclination angle is related to the "snubbing effect", owing to snubbing friction forces invoked by fiber bending. As illustrated in Fig. 10a, when a straight fiber is being pulled out from a matrix with an inclination θ under a force P, a snubbing friction force F will be generated by the normal force N and the relative slip between the fiber and matrix. In assumption that the matrix has the same deformation with the bending fiber in the curvature part, the friction system can then be illustrated as a tensioned fiber snubbed to a virtual cylinder [44]. This invoked snubbing friction force only exists in the curvature region and it can promote enhancements of the pullout resistance and the overall composite toughness [44,25]. In contrast, the "matrix spalling effect" will lead to the decrease of pullout load with the angle increment. Fiber inclination can cause a stress concentration at the matrix pullout surface, and consequently, local failure of the supporting matrix near the bearing point, i.e. matrix spalling occurs [17]. As the inclination angle increases, the stress concentration is also enhanced, leading to a more considerable portion of the concrete to crush at the pullout surface and a longer freed embedded length, thus a lower pullout load [26].

To study the snubbing effect and the matrix spalling effect, corresponding evaluation coefficients, i.e. snubbing friction coefficient f and spalling coefficient k, are calculated. It should be noted that previously proposed equations for calculating f were developed only for straight fibers without mechanical anchorage [17,26,28]. This study expands the equations for hooked end fibers and proposes a new analytical model.

Firstly, a normalized load is defined as the ratio of the peak load to the pullout length at a given angle θ, normalized with the ratio for the pullout angle of 0° [17]:

$$P_n = \frac{P_{max,\theta}/L_\theta}{P_{max,0}/L_0} \tag{4}$$

where $P_{max,\theta}$ and $P_{max,0}$ are the peak pullout loads of a straight or hooked end fiber under θ and 0° (MPa); L_θ and L_0 are the corresponding actual fiber embedded length (mm).

As suggested in [17,26,28,45], the following equation is used to represent the snubbing effect on straight fiber:

$$P_{n,s} = \frac{P_{max,s,\theta}/L_\theta}{P_{max,s,0}/L_0} = e^{f\theta} \tag{5}$$

in which $P_{n,s}$ is the normalized load for the straight fiber; $P_{max,s,\theta}$ and $P_{max,s,0}$ are the peak pullout loads of the straight fiber under θ and 0° (MPa), respectively.

Assuming that the interfacial shear stress is uniform along the embedded fiber and increases gradually with the pullout load until it approaches the interfacial shear strength τ_s [46], together with Eq. (5), $P_{max,s,\theta}$ and $P_{max,s,0}$ can be given as:

$$P_{max,s,0} = \pi d L_0 \tau_s \tag{6}$$

$$P_{max,s,\theta} = \pi d L_\theta \tau_s e^{f\theta} \tag{7}$$

Next, the above equations are expanded for hooked end fibers. The snubbing effects of the hooked end fiber under 0°and θ are shown in Fig. 10b and c, where α is the angle of the hook; L_{IJ} represents the length between point I and J, with $I, J = A$ to D. As can be observed, even when the hooked end fiber is aligned, snubbing friction forces will be generated during the pullout process because of the curvatures of the hook (the virtual cylinders in Fig. 10b). This denotes similar snubbing effects as the inclined straight fiber in Fig. 10a. Consequently, the peak pullout forces for the hooked end fiber under 0° and θ (MPa) can be expressed as Eqs. (8) and (9):

$$\begin{aligned} P_{max,h,0} &= \pi d L_{AB,0}\tau_s + \pi d L_{BC,0}\tau_s e^{f\alpha} + \pi d L_{CD,0}\tau_s e^{f\alpha} \\ &= \pi d L_{AB,0}\tau_s + \pi d L_{BD,0}\tau_s e^{f\alpha} \end{aligned} \tag{8}$$

$$\begin{aligned} P_{max,h,\theta} &= \pi d L_{AB,\theta}\tau_s e^{f\theta} + \pi d L_{BC,\theta}\tau_s e^{f\alpha} + \pi d L_{CD,\theta}\tau_s e^{f\alpha} \\ &= \pi d L_{AB,\theta}\tau_s e^{f\theta} + \pi d L_{BD,\theta}\tau_s e^{f\alpha} \end{aligned} \tag{9}$$

Substituting Eqs. (8) and (9) into Eq. (4), the normalized load for the hooked end fiber considering the snubbing effect is obtained:

$$P_{n,h,1} = \frac{P_{max,h,\theta}/L_\theta}{P_{max,h,0}/L_0} = \frac{(L_{AB,\theta}e^{f\theta} + L_{BD,\theta}e^{f\alpha})L_0}{(L_{AB,0} + L_{BD,0}e^{f\alpha})L_\theta} \tag{10}$$

Moreover, supposing that the pullout load does not reduce in the case of aligned fiber and that the pullout load does not act on the fiber when the load direction is perpendicular to the fiber axial, an equation to account for the spalling effect is presented [26,28]:

$$P_{n,h,2} = (\cos\theta)^k \tag{11}$$

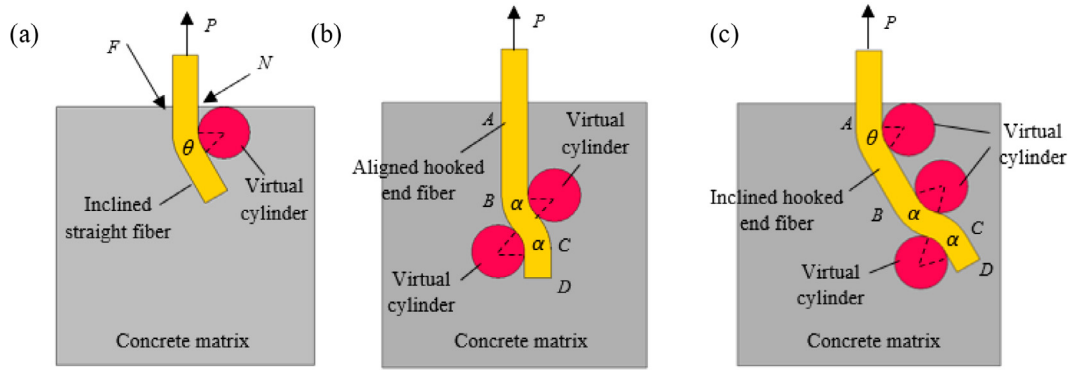

Fig. 10. Illustrations of snubbing effect: (a) inclined straight; (b) aligned hooked end; (c) inclined hooked end fibers.

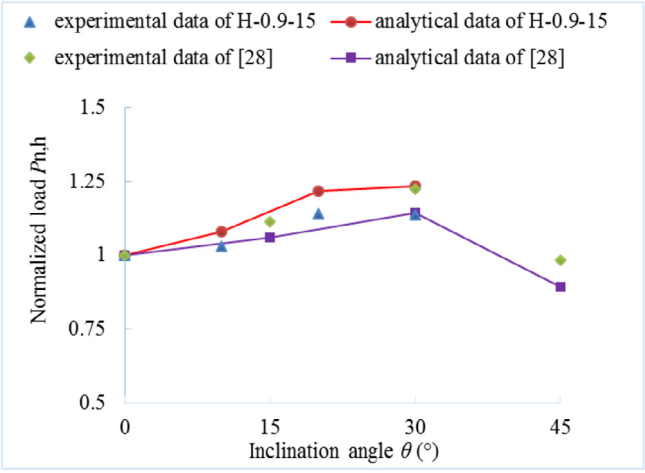

Fig. 11. Comparison between experimental data and analytical modelling.

Combining the above two effects, an analytical model for the hooked end fiber is proposed:

$$P_{n,h} = \frac{P_{max,h,\theta}/L_\theta}{P_{max,h,0}/L_0} = \frac{(L_{AB,\theta}e^{f\theta} + L_{BD,\theta}e^{f\alpha})L_0}{(L_{AB,0} + L_{BD,0}e^{f\alpha})L_\theta}(\cos\theta)^k \quad (12)$$

The results of the H-0.9-15 category are applied for validating the analytical model, with the angle of the hook $\alpha = 45°$; hook length $L_{BC} = 2.12$ mm and $L_{CD} = 2.5$ mm; $L_{AB} = L - L_{BC}sin\alpha - L_{CD}$. The obtained f and k are 1.25 and 1.0, respectively. Fig. 11 plots the comparison between the test results and the calculated normalized loads for the H-0.9-15 category, as well as for the pullout tests results in [28] with the above obtained f and k. The excellent match confirms the validity of the proposed model. It is noted that for the analytical results of [28], k is only used for the inclination case of 45°, in which concrete spalling was observed [28]. Besides, it should be aware that the obtained f and k in this study are distinct from the ones in [26] with straight steel fiber, i.e. $f = 1.6$, $k = 1.8$. This can be explained by the following reasons. Firstly, the test specimen in [26] includes 32 steel fibers, and the pullout behavior is examined using the average value relative to one fiber. This measure of the pullout load can differ with the result from a single fiber pullout test since it is almost impossible to achieve a uniform load distribution to all the fibers. Moreover, group effect appears in the multiple-fiber tests in [26], which may reduce the fiber efficiency as well as the matrix's capability to resist the bond [19]. Hence, the snubbing friction force has a distinct distribution in the fiber and the spalling of the matrix is also different.

5. Mesoscopic observations

Mesoscopic observations of the fibers after the pullout tests are performed by using an optical microscope to further investigate the effects of orientation angles on the fiber-matrix bond. The H-0.38-10 and the H-0.9-15 fibers before and after the pullout tests are compared and shown in Figs. 12 and 13. It is evident that the brass coating of the H-0.38-10 fiber is almost completely delaminated from the steel surface after the pullout test. This is different from the H-0.9-15 category, in which most of the coated brass still remains on the fiber surface. Thanks to the fine ingredients in the UHPC matrix, only a few longitudinal scratches due to matrix abrasion are observed on the surfaces of the pulled-out fibers. Furthermore, insignificant difference exists between the fiber surfaces under 0 and 30°: more matrix remnants are observed adhering to the fiber under 30°, e.g. Fig. 12c. These cementitious materials sticking to the fiber accumulate near the fiber end, which in turn are expected to enhance the friction in the post-peak pullout stage. This is in line with the slightly larger post-peak load for the H-0.38-10 fiber under 30° (see Fig. 6).

The fiber-matrix interfaces are also observed using SEM. The images of the microstructures around the H-0.38-10 fiber under 0° and 30° are presented in Fig. 14. Only a few pores are revealed in the interfacial transition zones (ITZ) around the fiber, implying a dense microstructure and a strong bond between the fiber and the UHPC matrix. This dense ITZ induces the delamination of the brass coating from the fiber surface during the pullout process and agrees well with the observations in Fig. 12. In addition, the similar ITZ for the 0 and 30° fibers indicates that the microstructure densification of ITZ is almost not influenced by the inclination angle. According to [30], the physico-chemical bond is one primary component of the fiber-matrix bond, and it is dependent on both the matrix packing density and fiber surface properties. The resemble ITZ density in Fig. 14 under different inclination angles reveals a similar physico-chemical bond between the fiber and the matrix, which also helps to explain the similar initial ascending slop of the pullout curves in Fig. 6 that is associated with the fiber-matrix adhesive bonding and debonding process.

6. Conclusions

The pullout performances of the hooked end steel fibers embedded in UHPC matrix are systematically investigated in this study. Two types of hooked end fiber with distinct fiber diameter and embedded length are tested and discussed. The effects of inclination angles (0°, 10°, 20° and 30°) on the pullout response are analyzed by the single fiber pullout tests, mechanical parameter calculations, mechanisms analysis and mesoscale observations. The following conclusions can be drawn from the study:

Due to the strong bond and anchorage in the UHPC matrix, the hooked end fiber with a small diameter, i.e. the H-0.38-10 fiber, ruptures prematurely under a large inclination angle. This is attributed to the fiber apparent strength degradation that increases with orientation. In contrast, the large fiber with an appropriate embedded length, i.e. the H-0.9-15 fiber, shows a complete pullout behavior and exhibits a more ductile response under the tested angles.

Embedded length is an important factor that affects the pullout response of the large hooked end fiber. In the H-0.9-10 category, the relatively small embedded length results in a serious matrix failure problem, which tremendously reduces the energy absorption capacity of the specimen. This phenomenon should be taken into account in design of UHPFRC composites.

For the H-0.38-10 category, the peak pullout loads are similar under various inclination angles, whereas it increases with the angle for the H-0.9-15 category. For the H-0.9-10 category, the optimum inclination

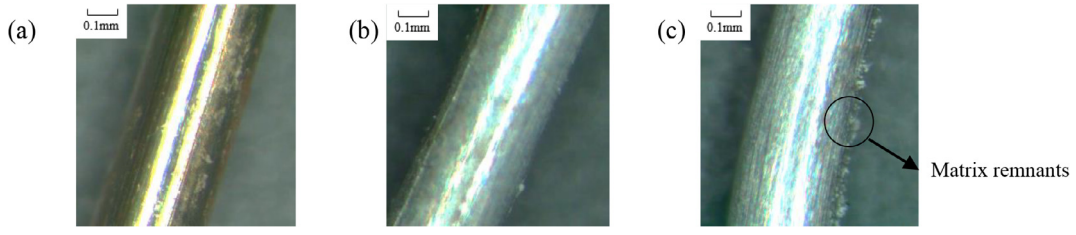

Fig. 12. H-0.38-10 fiber under optical microscope observation: (a) Before pullout test; (b) Pulled out under 0°; (c) Pulled out under 30°.

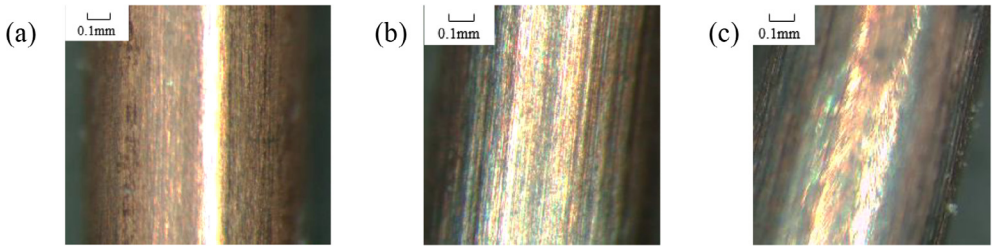

Fig. 13. H-0.9-15 fiber under optical microscope observation: (a) Before pullout test (b) Pulled out under 0° (c) Pulled out under 30°.

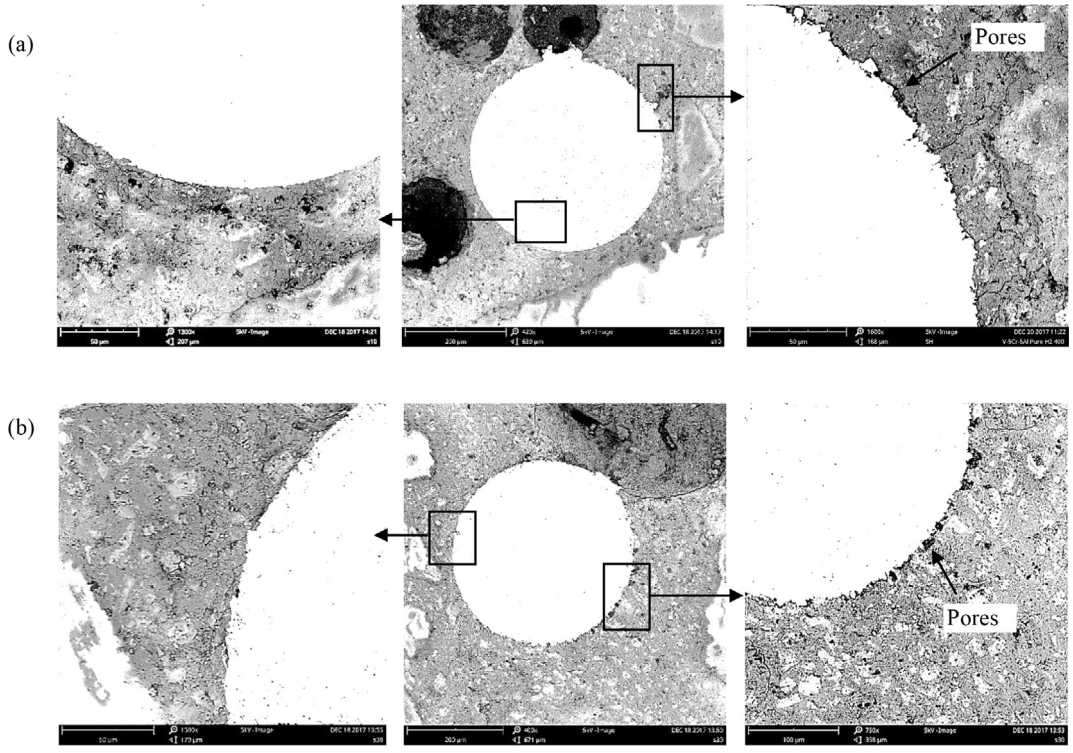

Fig. 14. SEM images of microstructures around H-0.38-10 fiber: (a) Inclination angle 0°; (b) Inclination angle 30°.

angle to achieve the maximum pullout resistance is around 20°.

Regarding fiber efficiency, the hooked end fiber with a small diameter, i.e. the H-0.38-10 fiber, has a higher utilization level and it is the highest under a pullout angle of 0°. The utilization efficiency for the H-0.9-10 and H-0.9-15 categories are approximately half of the H-0.38-10 category, and both of them reach the maximum values under 30°.

To effectively evaluate the combined effects of snubbing and matrix spalling, a new analytical model for hooked end fibers are proposed. It shows clearly that the analytical model provides a reasonable agreement with the experimental data.

The SEM images of the fiber-matrix interface confirm the dense microstructure of the ITZ in the designed UHPC matrix. It demonstrates that the fiber inclination do not have much influence on the densification of the ITZ, thus the physico-chemical bond between the fiber and the matrix.

Acknowledgements

This research was carried out under the funding of China Scholarship Council (No. 201503170258) and Eindhoven University of Technology. Mr. Verhagen is thanked for the experimental supports. Furthermore, the authors wish to express their gratitude to the following sponsors of the Building Materials research group at TU Eindhoven: Rijkswaterstaat Grote Projecten en Onderhoud; Graniet-Import Benelux; Kijlstra Betonmortel; Struyk Verwo; Attero; Enci; Rijkswaterstaat Zee en Delta-District Noord; Van Gansewinkel Minerals; BTE; V.d. Bosch Beton; Selor; GMB; Icopal; BN International; Eltomation, Knuaf Gips; Hess AAC Systems; Kronos; Joma; CRH Europe Sustainable Concrete Centre; Cement & Beton Centrum; Heros; Inashco; Keim; Sirius International; Boskalis; NNERGY; Millvision; Sappi and Studio Roex (in chronological order of joining).

References

[1] Yu R. Development of sustainable protective Ultra-High Performance Fiber Reinforced Concrete (UHPFRC)-Design, assessment and modeling {Ph.D. Thesis} Eindhoven, The Netherlands: Eindhoven University of Technology; 2015.
[2] Rossi P. Influence of fiber geometry and matrix maturity on the mechanical performance of ultra-high-performance cement-based composites. Cem Concr Compos 2013;37:246–8.
[3] Yu R, Spiesz PR, Brouwers HJH. Static properties and impact resistance of a green Ultra-High Performance Hybrid Fiber Reinforced Concrete (UHPHFRC): experiments and modeling. Constr Build Mater 2014;68:158–71.
[4] Yu R, Spiesz PR, Brouwers HJH. Mix design and properties assessment of Ultra-High-Performance Fiber Reinforced Concrete (UHPFRC). Cem Concr Res 2014;56:29–39.
[5] Tran NT, Tran TK, Jeon JK, Park JK, Kim DJ. Fracture energy of ultra-high-performance fiber-reinforced concrete at high strain rates. Cem Concr Res 2016;79:169–84.
[6] Hassan AMT, Jones SW, Mahmud GH. Experimental test methods to determine the uniaxial tensile and compressive behavior of Ultra-high Performance Fiber Reinforced Concrete (UHPFRC). Constr Build Mater 2012;37:874–82.
[7] Thomas J, Ramaswamy A. Mechanical properties of steel fiber-reinforced concrete. ASCE J Mater Civ Eng 2007;19(5):385–92.

[8] Johnston CD. Fiber-reinforced cements and concrete. Ottawa, Canada: Gordon and Breach Science Publishers; 2001.
[9] Tran NT, Tran TK, Kim DJ. High rate response of ultra-high-performance fiber reinforced concretes under direct tension. Cem Concr Res 2015;69:72–87.
[10] Wille K, Naaman AE. Bond Stress-Slip Behavior Of Steel Fibers Embedded In Ultra High Performance Concrete. Proceedings of 18th European conference on fracture and damage of advanced fiber-reinforced cement-based materials; 2010. 99–111.
[11] Abdallah S, Fan MZ, Zhou XM. Pullout behavior of hooked-end steel fibers embedded in ultra-high performance mortar with various W/B ratios. Int J Concr Struct Mater 2017;11(2):301–13.
[12] Markovic I. High-performance hybrid-fiber concrete - development and utilisation [Ph.D. Thesis]. Delft, The Netherlands: Technische Universiteit Delft; 2006.
[13] Orange G, Acker P, Vernet C. A new generation of UHP concrete: DUCTAL damage resistance and micromechanical analysis. Proc RILEM- High Perform Fiber Reinf Cem Compos 1999:101–11.
[14] Kim JJ, Kim DJ, Kang ST, Lee JH. Influence of sand to coarse aggregate ratio on the interfacial bond strength of steel fibers in concrete for nuclear power plant. Nucl Eng Des 2012;252:1–10.
[15] Park SH, Ryu GS, Koh KT, Kim DJ. Effect of shrinkage reducing agent on pullout resistance of high-strength steel fibers embedded in ultra-high-performance concrete. Cem Concr Compos 2014;49:59–69.
[16] Yoo DY, Park JJ, Kim SW. Fiber pullout behavior of HPFRCC: Effects of matrix strength and fiber type. Compos Struct 2017;174:263–76.
[17] Li VC, Wang Y, Backer S. Effect of inclining angle, bundling and surface treatment on synthetic fibre pull-out from a cement matrix. Composites 1990;21(2):132–40.
[18] Wille K, Naaman AE. Effect of ultra-high-performance concrete on pullout behavior of high-strength brass-coated straight steel fibers. Mater J 2012;110(4):451–62.
[19] Wille K, Naaman AE. Pullout behavior of high-strength steel fibers embedded in ultra-high-performance concrete. Mater J 2012;109(46):479–88.
[20] Wille K, Naaman AE. Ultra-high performance concrete and fiber reinforced concrete: achieving strength and ductility without heat curing. Mater Struct 2012;45(3):309–24.
[21] Yoo DY, Lee JH, Yoon YS. Effect of fiber content on mechanical and fracture properties of ultra high performance fiber reinforced cementitious composites. Compos Struct 2013;106:742–53.
[22] Laranjeira F, Molins C, Aguado A. Predicting the pullout response of inclined hooked steel fibers. Cem Concr Res 2010;40:1471–87.
[23] Isla F, Ruano G, Luccioni B. Analysis of steel fibers pull-out. Experimental study. Constr Build Mater 2015;100:183–93.
[24] Zhang J, Li VC. Effect of inclination angle on fiber rupture load in fiber reinforced cementitious composites. Compos Sci Technol 2002;62:775–81.
[25] Robins P, Austin S, Jones P. Pull-out behaviour of hooked steel fibres. Mater Struct 2002;35:434–42.
[26] Lee Y, Kang ST, Kim JK. Pullout behavior of inclined steel fiber in an ultra-high strength cementitious matrix. Constr Build Mater 2010;24:2030–41.
[27] Xu M, Hallinan B, Wille K. Effect of loading rates on pullout behavior of high strength steel fibers embedded in ultra-high performance concrete. Cem Concr Compos 2016;49:59–69.
[28] Tai YS, El-Tawil S. High loading-rate pullout behavior of inclined deformed steel fibers embedded in ultra-high performance concrete. Constr Build Mater 2017;148:204–18.
[29] Yoo DY, Banthia N. Mechanical properties of ultra-high-performance fiber-reinforced concrete: a review. Cem Concr Compos 2016;73:267–80.
[30] Wille K. Concrete strength dependent pull-out behavior of deformed steel fibers. In: 8th RILEM international symposium on fiber reinforced concrete: challenges and opportunities; 2012. p. 123–35.
[31] Peng Y, Wu H, Fang Q, Liu JZ, Gong ZM. Impact resistance of basalt aggregated UHP-SFRC/fabric composite panel against small caliber arm. Int J Impact Eng 2016;88:201–13.
[32] Tai YS, El-Tawil S, Chung TH. Performance of deformed steel fibers embedded in ultra-high performance concrete subjected to various pullout rates. Cem Concr Res 2016;89:1–13.
[33] Liu JZ, Han FY, Cui G, Zhang QQ, Lv J, Zhang LH, et al. Combined effect of coarse aggregate and fiber on tensile behavior of ultra-high performance concrete. Constr Build Mater 2016;121:310–8.
[34] Kim DJ, Park SH, Ryu GS, Koh KT. Comparative flexural behavior of Hybrid Ultra High Performance Fiber Reinforced Concrete with different macro fibers. Constr Build Mater 2011;25:4144–55.
[35] Yoo DY, Kim S, Park GJ, Park JJ, Kim SW. Effects of fiber shape, aspect ratio, and volume fraction on flexural behavior of ultra-high-performance fiber-reinforced cement composites. Compos Struct 2017;174:375–88.
[36] Wille K, Naaman AE, El-Tawil S, Parra-Montesinos GJ. Ultra-high performance concrete and fiber reinforced concrete: achieving strength and ductility without heat curing. Mater Struct 2012;45:309–24.
[37] Wille K, Kim DJ, Naaman AE. Strain-hardening UHP-FRC with low fiber contents. Mater Struct 2011;44:583–98.
[38] Park SH, Kim DJ, Ryu GS, Koh KT. Tensile behavior of ultra high performance hybrid fiber reinforced concrete. Cem Concr Compos 2012;34:172–84.
[39] Wu Z, Shi C, He W. Effects of steel fiber content and shape on mechanical properties of ultra high performance concrete. Constr Build Mater 2016;103:8–14.
[40] Li PP, Yu QL, Brouwers HJH. Effect of coarse basalt aggregates on the properties of Ultra-high Performance Concrete (UHPC). Constr Build Mater 2018;170:649–59.
[41] Banthia N, Trottier JF. Concrete reinforced with deformed steel fibers, part I: bond-slip mechanisms. ACI Mater J 1994;91(5):435–46.
[42] Kim DJ, El-Tawil S, Naaman AE. Loading rate effect on pullout behavior of deformed steel fibers. ACI Mater J 2008;105(6):576–84.
[43] Wu ZM, Shi CJ, Khayat KH. Influence of silica fume content on microstructure development and bond to steel fiber in ultra-high strength cement-based materials (UHSC). Cem Concr Compos 2016;71:97–109.
[44] Li VC, Wang Y, Backer S. A micromechanical model of tension-softening and bridging toughening of short random fiber reinforced brittle matrix composites. J Mech Phys Solids 1991;39(5):607–25.
[45] Yang EH, Wang SX, Yang YZ, Li VC. Fiber-bridging constitutive law of engineered cementitious composites. J Adv Concr Technol 2008;6(1):181–93.
[46] Fu SY, Zhou BL, Lung CW. On the pull-out of fibers with fractal-tree structure and the inference of strength and fracture toughness of composites. Smart Mater Struct 1992;1:18–185.